Exploring the VLBI Imaging Challenge: 6.819 Final Project

Jeffrey Basta
Massachussetts Institute of Technology
77 Mass. Ave, Cambridge, MA
jbasta@mit.edu

Ilona Demler
Massachussetts Institute of Technology
77 Mass. Ave, Cambridge, MA
ilonadem@mit.edu

Abstract

The paper explores different VLBI imaging algorithms on publicly available simulated Event Horizon Telescope Data. The current challenge consists in coming up with an optimal way to go from sparse measurements in the Fourier domain to the most likely source image in the image domain. We explore two such algorithms: our implementation of CLEAN, which provides a baseline for imaging techniques, and our spin on RML (regularized maximum likelihood). In our implementation of RML, we show that using closure phase data with a total variation denoising regularizer yields optimal results.

1. Introduction

Black holes are a difficult imaging task not only because they absorb all visible light, but because they are located at such great distances away from earth. For example, M87 is one of two black holes near Earth with the largest angular diameters. However, despite its massive shadow of 650 AU, the shadow that we observe is only 10^{-8} degrees because of its distance from earth [8].

$$d_{\text{shadow}} \approx 650 \text{ AU}$$

$$D_{\text{M87}} \approx 50,000,000 \text{ light years}$$

$$d_{\text{obs}} = \frac{d_{\text{shadow}}}{D_{\text{M87}}} = \frac{0.01}{5 * 10^6} \approx 10^{-8} \text{ deg}$$

At observable wavelengths, standard telescopes are not enough to resolve images of this size. Properly performing such a task requires a telescope about the size of the earth.

VLBI (very long baseline interferometry) is a technique developed to handle this problem [5]. It relies on combined measurements taken by arrays of telescopes positioned at distances away from each other around earth, and measures the Fourier components of the sky image on baselines between the telescopes [4]. This increases the resolving power of the data that is collected. The challenge of the black hole reconstruction problem is in interpreting the VLBI measurements to reconstruct an optimal image. More specifically, given a set of sparse measurements, there are infinitely many possible true images that could result in the data. There are not enough visibility measurements to simply do an inverse Fourier transform to get back the original image of the objects being observed. Therefore, we must rely on various imaging techniques in order to return our best approximation of the source image.

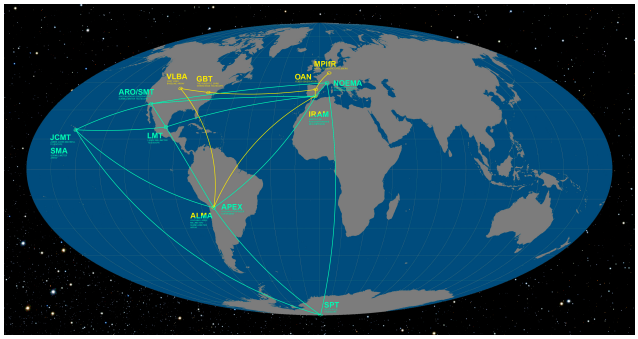

Figure 1. Event Horizon Telescope: network of radio telescopes around Earth which take VLBI measurements. Their combined array has sufficient angular resolution to resolve objects comparable in size to a supermassive black hole's event horizon [3]

.

1.1. Event Horizon Telescope (EHT)

The Event Horizon Telescope (Figure 1) is a network of radio telescopes stationed around the world which take VLBI measurements [10]. When combined together, they provide an angular resolution that is fine enough to make measurements of the event horizon of a black hole. In April of 2019, the EHT collaboration published the first ever image of a black hole using data measured from the supermassive black hole at the center of the Messier 87 Galaxy [9].

The telescopes collect visibilities, which are single complex Fourier components of the object image I, or a series of measurements (u, v) in the spatial frequency plane that are orthogonal to a telescope pair's line of sight [4]. As

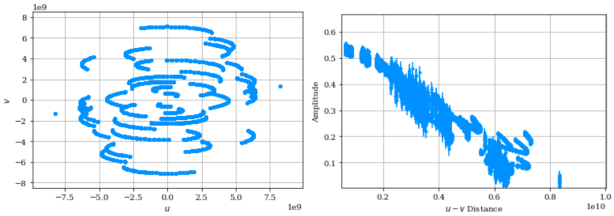

Figure 2. Left: Raw (u,v) data collected by telescopes. Right: interpolated visibilties

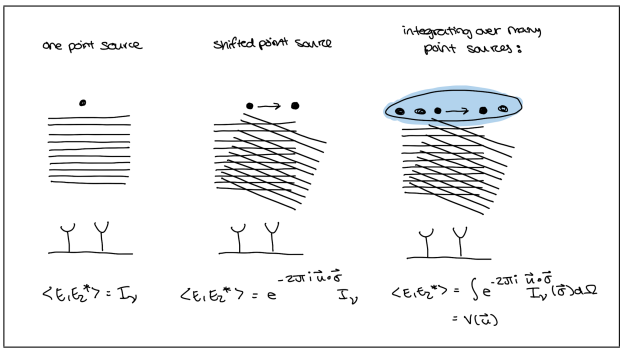

Figure 3. VLBI Measurements. The electromagnetic wavefront measured by the two telescopes from a signal emanating from a point source (left diagram) is equal to the intensity of that signal. If this signal were to shift (center diagram), then the electromagnetic wavefront would experience a phase shift corresponding to the shift and the distance between the two telescopes. We can therefore approximate large objects as a series of point sources, each of which emanates an EM-wavefront (right diagram) [4].

earth rotates, the baselines between telescopes rotate along with it, adding additional (u,v) measurements in the Fourier domain (Figure 2).

1.2. Very Long Baseline Interferometry (VLBI)

VLBI is a type of interferometry in which signals from astronomical radio sources are collected by multiple radio telescopes around earth. Alongside radio data, each antenna also records the time from a local atomic clock. The time difference in the arrivals of signals at each location is used to calculate the distance between radio telescopes. The data from different antennas in the array that record the same radio signal are correlated with each other in order to get the resulting image. Subsequently, this allows us to combine measurements to produce a result that would have been collected by a telescope of a size equal to the maximum separation between telescopes in the telescope array [5].

To foster a deeper understanding of this technique, we can first consider point sources (Figure 3). The electromagnetic wavefront measured by the two telescopes from a signal emanating from a point source is equal to the intensity

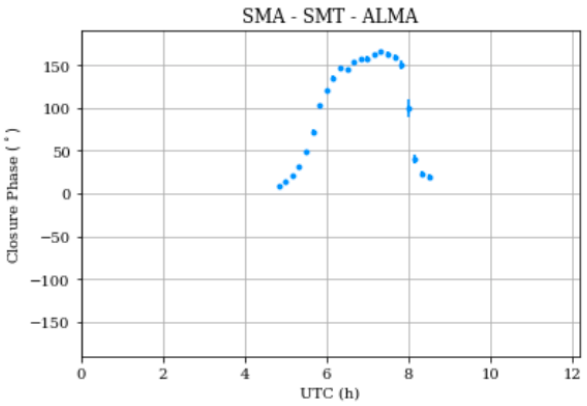

Figure 4. Closure phase measurements between SMA, SMT, and ALMA telescope sites. The closure phase is calculated by combining the pairwise visibilities across three sites.

of that signal. If this point source were to shift, then the electromagnetic wavefront measured by the two telescopes would undergo a phase shift.

Thus, we can consider the signal coming from a larger object as the result of integrating over many point sources. In other words, for a single wavelength λ, we can approximate the visibilities, or the time-averaged correlation of the measured signals from two telescopes, as the following integral (the van Cittert-Zernike Theorem [7]):

$$\Gamma_{i,j}(u,v) \approx \int_l \int_m e^{-i2\pi(ul+vm)} I_\lambda(l,m) dl dm \quad (1)$$

Where $I_\lambda(l,m)$ is the emission at wavelength λ, (u,v) are dimensionless coordinates measured in wavelengths, and $\Gamma_{i,j}(u,v)$ is the visibility measurement. It is immediately noticeable that this form is identical to that of the Fourier transform of the source image $I_\lambda(l,m)$. Thus, the combined measurement $\Gamma_{i,j}(u,v)$ from two telescopes is a single complex Fourier component of the source image at position (u,v) in the spatial frequency plane [4].

1.3. Closure Phase

We encounter an additional hurdle when we consider the atmospheric inhomogeneities that cause delays in the signals received by each telescope. We can approximate this with an additional phase term [4, 7]:

$$\Gamma_{i,j}^{meas} \approx e^{i(\phi_i - \phi_j)} \Gamma_{i,j}^{ideal} \quad (2)$$

where ϕ_i and ϕ_j are the phase shifts that are introduced to telescopes i and j, respectively.

Using this formulation and combining the visibilities of three telescopes ($\Gamma_{i,j}$, $\Gamma_{j,k}$, $\Gamma_{k,i}$) we get an expression that doesn't depend on the individual phase terms (ϕ_i, ϕ_j, ϕ_k)

of each telescope:

$$\Gamma^{meas}_{i,j}\Gamma^{meas}_{j,k}\Gamma^{meas}_{k,i} = e^{i[(\phi_i-\phi_j)+(\phi_j-\phi_k)+(\phi_k-\phi_i)]} * \Gamma^{ideal}_{i,j}\Gamma^{ideal}_{j,k}\Gamma^{ideal}_{k,i} \quad (3)$$

and therefore:

$$\Gamma^{meas}_{i,j}\Gamma^{meas}_{j,k}\Gamma^{meas}_{k,i} = \Gamma^{ideal}_{i,j}\Gamma^{ideal}_{j,k}\Gamma^{ideal}_{k,i} \quad (4)$$

The triple product of visibilities is also referred to as the bispectrum. It is a powerful set of measurements because it is independent of atmospheric effects. However, it also greatly reduces the amount of measurements that we make in the Fourier domain (since we must now consider all possible triple pairs of telescopes instead of all possible pairings). An example of closure data is displayed in Figure 4.

1.4. The Fourier Domain

Therefore, the imaging problem is as follows: given a sparse set of measurements in the Fourier domain, determine a mapping that returns an optimal reconstruction in the image domain. If we were to sample from the Fourier domain completely (i.e. if the earth were covered in telescopes), then this problem would simply require taking the inverse Fourier transform of the measurements.

Here, it is useful to define some terminology. The "dirty beam" is the inverse Fourier transform of the (u,v) measurements [6]. We sample the Fourier domain at discrete points:

$$B(u,v) = \sum_k (u_k, v_k)$$

the dirty image $T^D(x,y)$ is then defined as:

$$T^D(x,y) = FT^{-1}[B(u,v) \times V(u,v)]$$

where $V(u,v)$ is the 2D Fourier transform of the brightness on the sky, $T(x,y)$. From the convolution theorem we get that

$$T^D(x,y) = b(x,y) \otimes T(x,y)$$

where $b(x,y)$ is the point spread function:

$$b(x,y) = FT^{-1}[B(u,v)]$$

The "dirty image" is the true image convolved with the "dirty beam". In other words, we have that the Fourier transform of the sampled visibilities gives us the true sky brightness convolved with the point spread function [1]. Our goal is to recover the true sky image.

2. Related Work

There are several significant algorithms that have been attempted by other groups to solve the celestial imaging problem.

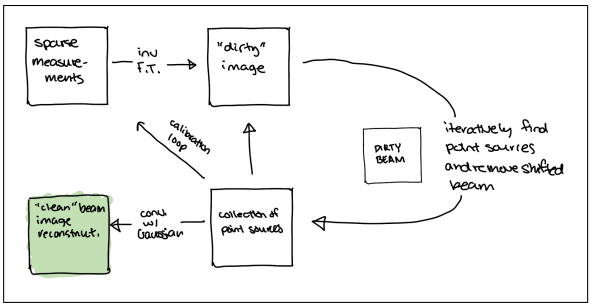

Figure 5. CLEAN algorithm outline

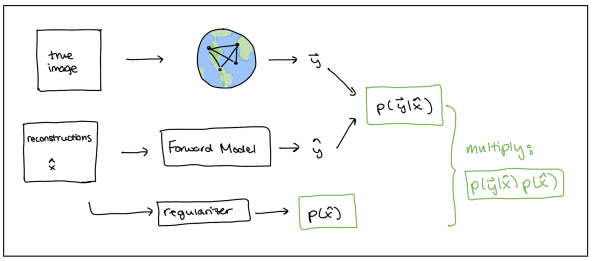

Figure 6. RML algorithm outline

2.1. CLEAN (Högbom)

This is a deconvolution algorithm that has been used for image reconstruction in the field of radio astronomy since 1974, when it was first published by Jan Hogbom [6]. It is both fast and yields clean results, and has seen widespread use in radioastronomy imaging problems .

The CLEAN algorithm iteratively looks for regions with the highest pixel intensities and deconvolves around those points. The result of this is a collection of point sources that fit the data. In order to make this result interpretable to humans, this collection of points is convolved with a "clean" beam (in our case an elliptical Gaussian fitted to the central lobe of the dirty beam). An outline of this framework is shown in figure 5.

2.2. Regularized Maximum Likelihood

This algorithm takes a Bayesian Model Inversion approach, taking advantage of the fact that there are infinitely many images that give the same sparse sampling in the Fourier domain. We take any image from this set of possible images (x) and evaluate it by running it through a forward model to generate synthetic data (y). We then calculate the probability of the actual observed data coming from this synthetic reconstruction. We can also add an additional prior term that evaluates this prior image distribution $P(x)$. This method is powerful because we can incorporate different effects (atmospheric pressure, systematic gain errors, thermal noise) into the calculation. An outline of this framework is shown in Figure 6.

The RML approach is a very general one, as such, there are several versions of it which perform quite well:

- BSMEM: uses a flat image prior and a maximum entropy prior. The optimal reconstruction image is found by using gradient descent optimization [2].
- SQUEEZE: uses MCMC to sample images from a posterior distribution. Images are then sampled by moving around the field of view, and the final image is calculated as the average of these samplings [11].

2.3. CHIRP

This is a novel Bayesian algorithm proposed by Bouman et al in 2017 which has seen significant results [8]. It approximates an image as a discrete number of scaled and shifted continuous pulse functions, and uses the expected patch log likelihood in constructing a maximum a posteriori estimate of image coefficients. It uses bispectrum measurements in order to counter atmospheric effects, and an expected patch log-likelihood to regularize the solution image. Algorithm optimization is done using "half quadratic splitting".

3. Approach/Algorithm

In this report we implement two algorithms for visualizing VLBI data: CLEAN and RML. For CLEAN, we implement the algorithm according to Högbom's original formulation [6]. For RML, we design an algorithm motivated by the efficacy of certain techniques in the CHIRP implementation [7].

3.1. Datasets

For the majority of our experiments we will be using simulated data from the VLBI imaging website (available at http://vlbiimaging.csail.mit.edu/). This simulation software was developed by Bouman et al. for the purpose of evaluating and comparing the performance of different image reconstruction algorithms. The idea behind the synthetic data is to start with known images and then sparsely sample from them in order to construct a dataset of images that would have been collected by the Event Horizon Telescopes. By training an algorithm that can correctly reconstruct the original training image from these sparse measurements, we can then use it to image real VLBI data. The majority of our experiments are conducted on the static black hole training dataset (staticBlackhole) and the M87 training dataset [7].

All datasets file the .OIFITS data file format. Based on the FITS standard, it is the standard for exchanging data for Optical (Visible/IR) Interferometry.

3.2. The ehtim library

The ehtim Python library was developed by Andrew Chael and is publicly available at (https://github.com/achael/eht-imaging). It contains several modules for simulating and manipulating VLBI data, as well as methods for producing images with regularized maximum likelihood methods [3]. We used this python library for three purposes:

1. reading in .OIFITS files
2. calculating the dirty image, dirty beam, and clean beam
3. helper functions when implementing RML

3.3. CLEAN implementation

We followed Högbom's formulation of the CLEAN algorithm [6]. The steps can be summarized as follows:

1. Find the strength and position of the peak in the dirty image
2. At the position of the peak, subtract the dirty beam multiplied by the peak strength and a damping factor
3. Return to (1) unless there are no remaining peaks above a user-specified level
4. Convolve the resulting point-source model with an idealized 'clean' beam (in our case an elliptical Gaussian fitted to the central lobe of the dirty beam)
5. Add the residuals of the dirty img to the 'clean' img

3.4. RML Implementation

In our implementation of RML we use the chi-squared goodness-of-fit metric. We also add a regularizer which penalizes the images that don't fit the criteria we need. There were two regularizers that we tried: an l1 norm, which encouraged sparsity in pixels, and total variation denoising (TV), which encouraged sparsity in the gradient.

We also tried out two different discrete Fourier transform packages: a python-defined "fast" fourier transform, which is faster but ended up compromising on result accuracy [3], and the pynfft library, which is a library for computing discrete Fourier transforms built on C [12].

Since the Bouman et. al results demonstrated that bispectral data (closure phases) performed significantly better than just visibilities, we also implemented this RML algorithm on bispectral data.

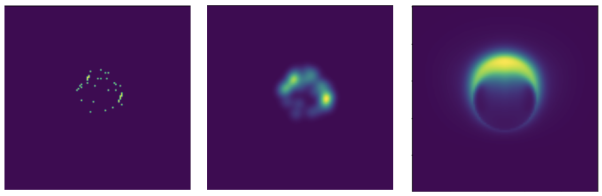

Figure 7. CLEAN Imaging results. Leftmost image shows the collection of point sources identified by the deconvolution and peak searching steps. Middle image shows these points convolved with a clean beam. Rightmost image is the ground truth. These pictures were generated from the synthetic staticBlackhole dataset.

4. Experimental Results

4.1. CLEAN Algorithm

Our implementation of the CLEAN algorithm was by far the fastest to run (results displayed in Figure 7). However, we were constrained by the number of pixels in our approximated image, and could therefore only find a finite number of peaks (ideally, if the image were infinitely large and the algorithm could run for infinitely many iterations we would be able to perfectly reconstruct the source image). We used these images as the baseline for our later experiments. Thus, even though the beams that we found corresponded to beams in the ground truth image, there weren't sufficiently many in order to reconstruct the original image to a reasonable degree.

4.2. Comparing Fourier transform methods

The results of RML using different Fourier transform methods are shown in Figures 8 and 9. The results are fairly comparable, with pynfft yielding lower chi-squared values than the fast Fourier transform. This is to be expected, since the pynfft library is more exact than the fast Fourier transform is. The ground truth image for both of these trainings is shown in Figure 13 on the right.

4.3. Visibilities vs. Bispectrum Measurements

Besides the chi-squared metric, another way to evaluate our image reconstructions is by comparing the visibilities and phase amplitudes reconstructed by our RML model. In Figure 10 we plot the amplitude and phase of the signals of the reconstructed signals and true signals. While most of the model shape is captured correctly, there are still points where it is not perfect.

From the graphs it is clear that using closure phases yields much more accurate results, however we also note that the data is much more sparse in this case (since there are less points when we consider N choose 3 instead of N choose 2 telescope combinations). Figures 12 and 13 show the RML algorithm using closure data on the static black

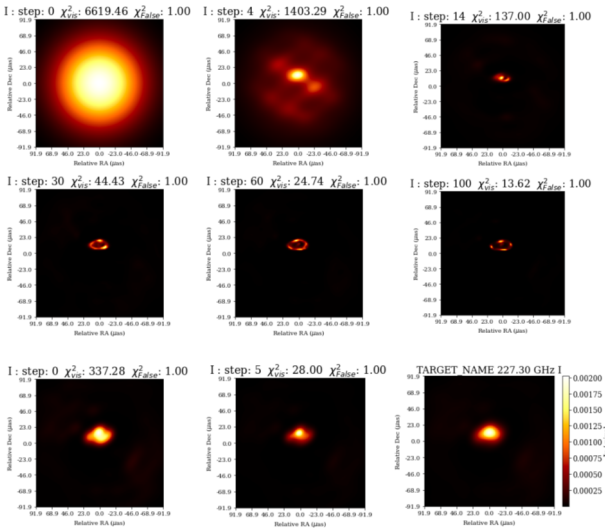

Figure 8. RML imaging algorithm using pynfft Fourier transform library. Top left image shows the Gaussian prior. The first two rows show one run of the training. The resulting beam (rightmost center image) is then convolved with the Guassian prior to prevent us from getting stuck in a local minimum, and we resume the algorithm from the start. The final image is shown in the bottom right.

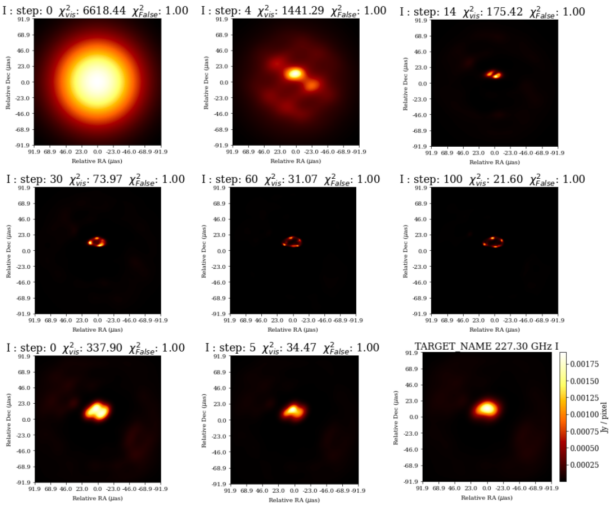

Figure 9. RML imaging algorithm using fast Fourier transform. Images follow the same pattern as in Figure 8, with the final resulting image shown in the bottom right.

hole as well as M85 simulated datasets, with the ground truth for each respective case being the rightmost image.

4.4. Comparing regularizers in RML algorithm

Additionally, we tested different regularizers with RML (results in table 1). Both regularizers improve between runs 1 and 3, but it looks like the TV regularizer yields better

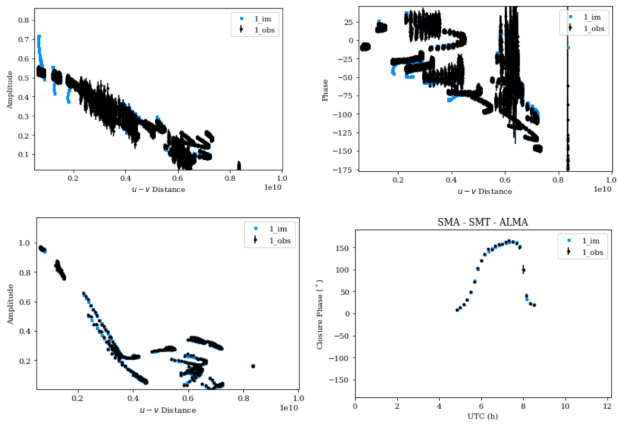

Figure 10. Phase and amplitude measurements, as generated by forward RML model (black) and ground truth from simulation data (in blue) with the pynfft package. Top row shows visibilities and bottom row shows closure phases (triple products of visibilities). Closure phase eliminates the effects of phase gains due to local noise, and results in a much cleaner fit.

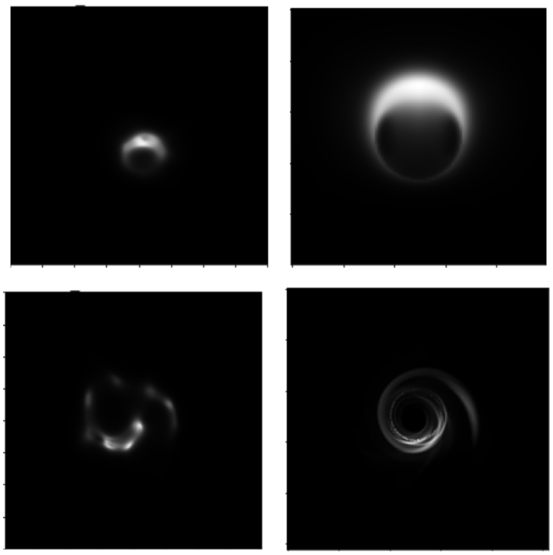

Figure 11. RML reconstructions. Right hand images are ground truth. Top row: RML algorithm with TV regularization and fast fourier transform. Note that the two images are not scaled similarly, which is why they two circles appear of different size. Bottom Row: left two images show RML image reconstructions, left with TV regularization and middle with l1.

results for the chi-squared values of the phase and the l1 regularizer yeilds better results for the chi-squared values of the amplitude. This result makes intuitive sense: TV should encourages sparsity in the gradient whereas l1 encourages sparsity in the pixels. So L1 should be better at matching the amplitudes of the images, whereas TV should be better at matching the phases.

Reg	χ^2_{cphase} (run1)	χ^2_{cphase} (run3)	χ^2_{amp} (run1)	χ^2_{amp} (run3)
TV	0.89	0.81	1.71	1.40
L1	1.02	0.88	1.46	1.27

Table 1. Comparison of regularization methods on static black hole reconstruction using 3 runs of successive image reconstruction and re-convolving with a Gaussian.

5. Conclusions

VLBI makes much progress in solving the problem of resolving prohibitively small objects in the night sky. By combining measurements from telescopes situated all around earth, we can get measurements of resolutions equal to those measured by the maximum distance between each set of telescopes. The telescopes collect visibilities, which are single complex Fourier components of the object image. However, the question still remains of how to best convert from these sparse sets of measurements in the Fourier domain to the true image.

In this paper we implement two algorithms for VLBI imaging techniques: CLEAN and RML. RML immedeately outperformed the CLEAN algorithm, as expected. We found that in all our experiments, using closure phases produced better results than simply the visibilities, because closure phases are independent of atmospheric contributions around each individual telescope. We also introduced two different regularizers for our RML model, l1 (which encouraged sparsity in the pixels) and TV (which encouraged sparsity in the gradient) and found that the quality of results varied depending on if we wanted to get the best phase or amplitude information. This result is further confirmed by plotting phase and amplitude measurements of the observed and interpolated results, with the bispectral data producing much cleaner matches to the data than the visibilities alone.

The open question remains of whether using correlation data between telescopes is truly sufficient evidence that the object being resolved is a black hole, but this is a question that goes beyond the scope of VLBI alone. In the future, we would like to combine the image parametrization as introduced by Bouman et al. [7] in our RML algorithm, to test whether it yields better calibration results. We would also want to experiment with different prior distributions, as well as different metrics besides chi-squared for evaluating the goodness-of-fit.

5.1. Partnered Work Breakdown

Although most work was done collaborativley, Jeff built the main body of CLEAN and Ilona built the main body of RML. Both worked on making RML compatible with phase closure data, and ran tests on different datasets.

References

[1] Jim Braatz. *Imaging: NAASC data analysis workshop*, 2015. 3

[2] D. Buscher. Direct maximum-entropy image recon- struction from the bispectrum. in very high angular resolution imaging. *Springer*, pages 91–93, 1994. 4

[3] Andrew Chael. ehtim python library. *github*, 15(1):417, 2011. 1, 4

[4] Andrew Chael. *VLBI Data Series 3: Imaging Techniques*, 2020. 1, 2

[5] C. L. Carilli G. B. Taylor and R. A. Perley. Synthesis imaging in radio astronomy. *Synthesis Imaging in Radio Astronomy*, 2, 1999. 1, 2

[6] Jan Högbom. Aperture synthesis with a non-regular distribution of interferometer baselines. *Astronomy and Astrophysics Supplement*, 15(1):417, 2011. 3, 4

[7] Daniel Zoran Vincent Fish Sheperd Doeleman William Freeman Katherine Bouman, Michael Johnson. Computational imaging for vlbi reconstruction. 2, 4, 6

[8] Jeremy Murphy, Karl Gebhardt, and Joshua Adams. Galaxy kinematics with virus-p: The dark matter halo of m87. *The Astrophysical Journal*, 729(2):129–150, 2011. 1, 4

[9] Luciano Rezzolla Prashant Kocherlakota and Event Horizon Telescope Collaboration. Constraints on non-einsteinian black-hole charges with the 2019 eht observations of m87. *Physical Review*, 103(10):40–47, 2019. 1

[10] D. E. Schenck C. Beau-doin R. Blundell G. C. Bower A. E. Broderick R. Chamberlin R. Freund P. Friberg et al. S. S. Doeleman, V. L. Fish. Jet- launching structure resolved near the supermassive black hole in m87. *Science*, 2012. 1

[11] M. Bremer W. Alef A. Witzel J. Zensus T. Krichbaum, D. Graham and A. Eckart. Submilliarcsecond imaging of sgr a* and m 87. *Journal of Physics: Conference Series*, IOP Publishing:91–93, 2006. 4

[12] Ghislain Vaillant. *fast fourier transform library*, 2019 [Online]. 4